

## Theoretical investigation of the negative differential resistance in squashed C60 molecular device

Zhi-Qiang Fan, Ke-Qiu Chen, Qing Wan, B. S. Zou, Wenhui Duan et al.

Citation: *Appl. Phys. Lett.* **92**, 263304 (2008); doi: 10.1063/1.2952493

View online: <http://dx.doi.org/10.1063/1.2952493>

View Table of Contents: <http://apl.aip.org/resource/1/APPLAB/v92/i26>

Published by the AIP Publishing LLC.

---

### Additional information on *Appl. Phys. Lett.*

Journal Homepage: <http://apl.aip.org/>

Journal Information: [http://apl.aip.org/about/about\\_the\\_journal](http://apl.aip.org/about/about_the_journal)

Top downloads: [http://apl.aip.org/features/most\\_downloaded](http://apl.aip.org/features/most_downloaded)

Information for Authors: <http://apl.aip.org/authors>

## ADVERTISEMENT



# Theoretical investigation of the negative differential resistance in squashed $C_{60}$ molecular device

Zhi-Qiang Fan,<sup>1</sup> Ke-Qiu Chen,<sup>1,a)</sup> Qing Wan,<sup>1</sup> B. S. Zou,<sup>1</sup> Wenhui Duan,<sup>2</sup> and Z. Shuai<sup>3</sup>

<sup>1</sup>Key Laboratory for Micro-Nano Optoelectronic Devices of Ministry of Education and Department of Applied Physics, Hunan University, Changsha 410082, People's Republic of China

<sup>2</sup>Department of Physics, Tsinghua University, Beijing 100084, People's Republic of China

<sup>3</sup>Key Laboratory of Organic Solids, Institute of Chemistry, Chinese Academy of Sciences, Beijing 100080, People's Republic of China

(Received 22 April 2008; accepted 6 June 2008; published online 2 July 2008)

By applying nonequilibrium Green's function and first-principles calculation, we investigate the transport behavior of squashed  $C_{60}$  molecular devices. The results show that the electronic transport properties are affected obviously by the deformation of  $C_{60}$  molecule. Negative differential resistance is found in such system and can be tuned by the deformation degree of the molecule. A mechanism for the negative differential resistance behavior is suggested. © 2008 American Institute of Physics. [DOI: 10.1063/1.2952493]

In recent years, progress in microfabrication and self-assembly techniques<sup>1</sup> have made it possible to design single molecular device. The electronic transport properties in single molecular junctions or molecular devices have attracted much attention. The current-voltage ( $I$ - $V$ ) characteristics of many molecular devices have shown interesting physical properties, including single-electron characteristics,<sup>2</sup> negative differential resistance (NDR),<sup>3</sup> electrostatic current switching,<sup>4</sup> etc. The most prominent among these effects is the NDR behavior due to its wide range of applications including amplification, logic, and memory, as well as fast switching. NDR behavior has been found in many physical systems such as double quantum wells,<sup>5</sup> superlattices,<sup>6,7</sup> and one-dimensional system.<sup>8</sup> It has also been found in a variety of molecular devices such as oligo(phenylene ethynylene) (OPE) molecular junctions,<sup>3,9-11</sup> bilayer OPE molecular junctions,<sup>12</sup> single benzene ring with a nitro-side group,<sup>13,14</sup> organometallic molecular double-dot system,<sup>15</sup> cobalt phthalocyanine molecule on a gold substrate,<sup>16</sup> the mirror symmetrical straight carbon-nanotube heterojunctions with different sizes and lengths,<sup>17</sup> etc. Possible mechanism such as a two-step reduction process,<sup>3</sup> the change in the molecular conformation due to the change in the electronic charge state of the molecule under increasing bias,<sup>9</sup> bias-induced alignment of molecular orbitals,<sup>10</sup> the rotation of the ligand activated by temperature,<sup>13</sup> local orbital symmetry matching between electrodes and molecule,<sup>16</sup> and the channel conduction being suppressed at a certain bias<sup>17</sup> have been proposed to explain the NDR behavior.

In the present work, by applying a first-principles computational method based on the density functional theory in combination with the nonequilibrium Green's functions theory, we investigate the electronic transport properties of squashed  $C_{60}$  molecular device. Ever since its discovery,<sup>18</sup>  $C_{60}$  molecule has attracted much attention because of its unique geometry, mechanical and chemical robustness, and extraordinary physical properties and potential application in nanotechnology. For this special structure, the adsorption of the ideal  $C_{60}$  molecule on metal electrodes has been studied

experimentally<sup>19-21</sup> and theoretically.<sup>22-24</sup> Joachim and co-workers found that the current-voltage characteristics present a linear behavior at a low applied bias voltage and squeezing a  $C_{60}$  molecule by applying a small force with a metallic scanning tunnel microscope tip can result in a shift of the molecular orbital levels.<sup>19,25</sup> Zeng *et al.* found NDR behavior in  $C_{60}$  molecular junction.<sup>21</sup> The present study is aimed at searching the deformation effects of the  $C_{60}$  molecule on NDR behavior of the molecular devices.

The  $C_{60}$  molecular device we study is illustrated schematically in Fig. 1. The system was divided into three regions: the left and right electrodes and the central scattering region. The distance between two electrodes is 12.373 Å, which is a typical distance employed in most of the

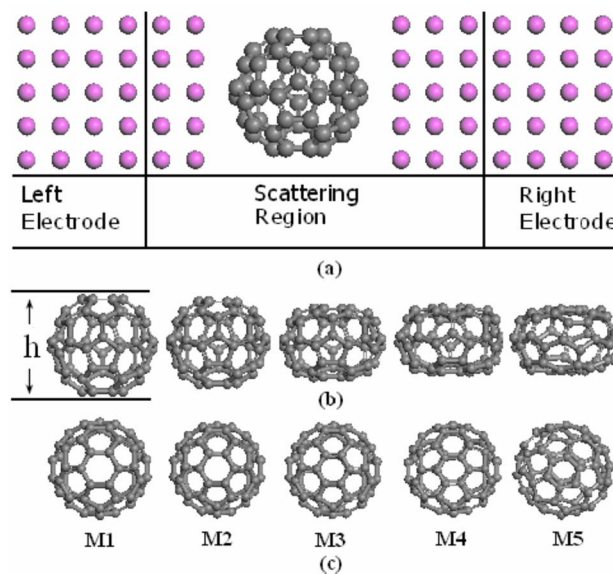


FIG. 1. (Color online) (a) Schematic description of the single  $C_{60}$  molecular device: the  $C_{60}$  molecule coupled to two semi-infinite Al electrodes, and the extended molecule consists of  $5 \times 5$  (100) three layers of Al slab with 38 atoms per unit cell in the right lead, two layers of Al slab with 25 atoms in the left lead. (b) Schematic description of the squashed  $C_{60}$  molecules. M1–M5 correspond to the distance between two parallel planes on the top and bottom  $h=6.7$  (ideal), 6.0, 5.0, 4.5, and 4.4 Å, respectively. (c) is the corresponding top views of M1–M5 shown in (b).

<sup>a)</sup> Author to whom correspondence should be addressed. Electronic mail: keqiu.chen@hnu.cn.

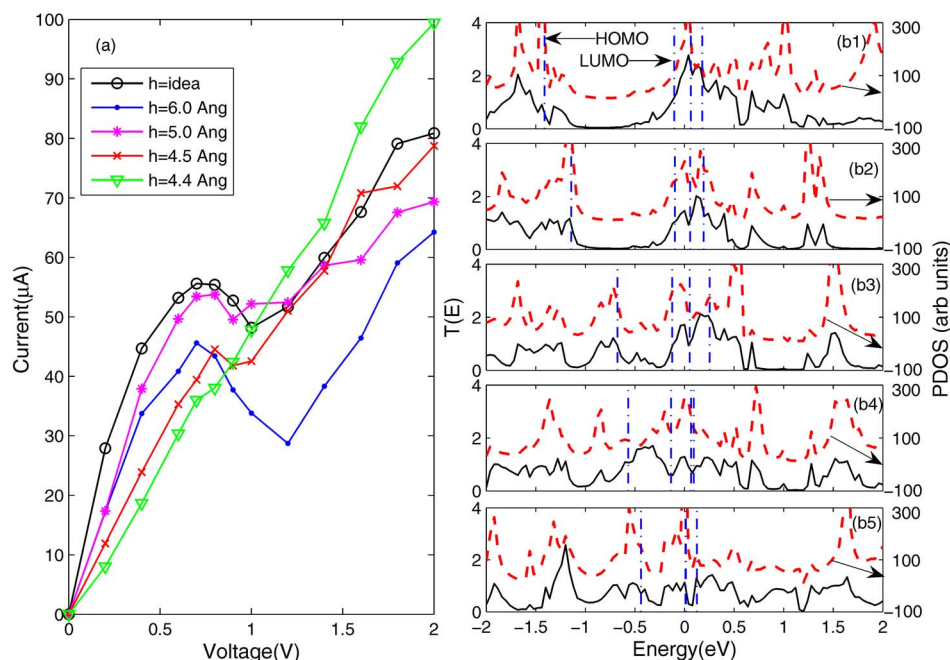


FIG. 2. (Color online) (a) Calculated current as a function of the applied bias for the single  $C_{60}$  molecular device with different  $h$ . (b1)–(b5) describe the transmission coefficient and the corresponding projection of the density of states (PDOS) for the systems  $M1$ – $M5$ , respectively. The vertical dash-dotted lines stand for the molecular orbitals, and the Fermi levels is set to be the origin of energy.

reference.<sup>20,24</sup> By using the Forcite modules of MATERIAL STUDIO software, the  $C_{60}$  molecule is compressed along the  $Y$ -axis and  $h$  is the distance between two parallel planes on the top and bottom, as shown in Fig. 1(b). The systems  $M1$ – $M5$  correspond to  $h = 6.7$  (no deformation),  $h = 6.0$ ,  $5.0$ ,  $4.5$ , and  $4.4 \text{ \AA}$ , respectively. Although  $M5$  is of only  $0.1 \text{ \AA}$  in  $h$  different from  $M4$ , the structure of  $M5$  is different from the other four structures. For  $M1$ – $M4$ , two parallel planes on the top and bottom is of hexagon-to-hexagon order, while for  $M5$ , the hexagons shift a little and do not remain to be face-to-face. This structural difference means that the electronic properties may be much more different from other four cases. The quantum transport calculations have been carried out by an *ab initio* code package, TRANSIESTA-C, developed by Brandbyge *et al.*<sup>26</sup>

In Fig. 2(a), we describe the current as a function of the applied bias voltage for all five systems. It is well known that the isolated pristine  $C_{60}$  molecule is a semiconductor and has a filled highest occupied molecular orbital (HOMO) and an empty threefold degenerate lowest unoccupied molecular orbital (LUMO). However, from the  $I$ - $V$  characteristic curves shown in Fig. 2(a),  $C_{60}$  molecular junction shows the metal behavior. This is due to the interaction between the  $C_{60}$  molecule and the metal electrodes, which typically results in electrons doped into the  $C_{60}$  molecule. From Fig. 2(a), it can be found that at low bias voltages, the current-voltage curve displays a linear behavior, which is in agreement with the experimental results reported by Joachim *et al.*<sup>19</sup> When the bias voltage is increased to a certain range, except the current of  $M5$  continues to increase, the current of the other systems steeply decreases almost at the same bias voltage and NDR appears. The peak-to-valley ratios are 1.154, 1.588, 1.085, and 1.065 corresponding to  $M1$ – $M4$ , respectively. This indicates that when the compression on the  $C_{60}$  molecule is reinforced, the NDR behavior is first intensified then bated and disappeared at last.

To explain the origin of the transport characteristics of the molecular junctions, in Figs. 2(b1)–2(b5), we give the transmission coefficient  $T(E, V_b)$  and the corresponding projection of the density of states (PDOS) at zero bias ( $V_b = 0$ )

for  $M1$ – $M5$  given in Fig. 1. From Fig. 2(b1), we find that three lowest unoccupied molecular orbitals, LUMO, LUMO+1, and LUMO+2, lie beside the Fermi energy level. This indicates that the electronic transport at low bias voltage is mainly contributed by the three LUMOs. The existence of the transmission peaks near the Fermi energy level also shows the metal behavior of the devices at small biases. These results are in agreement with the result obtained from analysis of the equilibrium transmission eigenvalues by Taylor *et al.*<sup>22</sup> Compare Fig. 2(b2) with Fig. 2(b1), it can be found that the small deformation of  $C_{60}$  seems not to affect the energy position of the three LUMOs of  $M2$ . However, the HOMO shifts obviously to the Fermi energy level. The average transmission coefficient of Fig. 2(b2) is smaller than that of Fig. 2(b1); in other words, the electronic transfer ability of the device weakens when the  $C_{60}$  molecule is squeezed. It is known that the transport coefficient is related to the wave function overlap between molecules and electrodes, namely, the coupling degree between molecular orbitals and the incident states from the electrodes. From  $M1$  to  $M2$ , the electronic transfer ability getting weaker should result from the decrease in the coupling degree between the electrodes and the molecule. From Fig. 2(b3), we can see clearly that when the molecule is further squashed, the HOMO further shifts toward the Fermi energy level and begins to make contribution to the current at low bias voltages. However, the LUMO+2 orbital shifts toward the higher energy region. From Figs. 2(b1) and 2(b2), a wide valley with very small transmission coefficient in the energy region between HOMO and LUMO for both systems  $M1$  and  $M2$  is seen clearly, but in Fig. 2(b3), the wide transmission valley disappears, instead several transmission peaks appear in the energy region. When compression of the  $C_{60}$  molecule continues, the transmission spectra maintain the foregoing variational trend, except the LUMO+2 shifting to approach the LUMO+1, as seen in Fig. 2(b4). However, from Fig. 2(b5), it can be found that both LUMO and LUMO+1 approach each other and seem to be degenerate, and they lie on the right of Fermi energy level, which is significantly different from the cases of the systems  $M1$ – $M4$ . The transmission

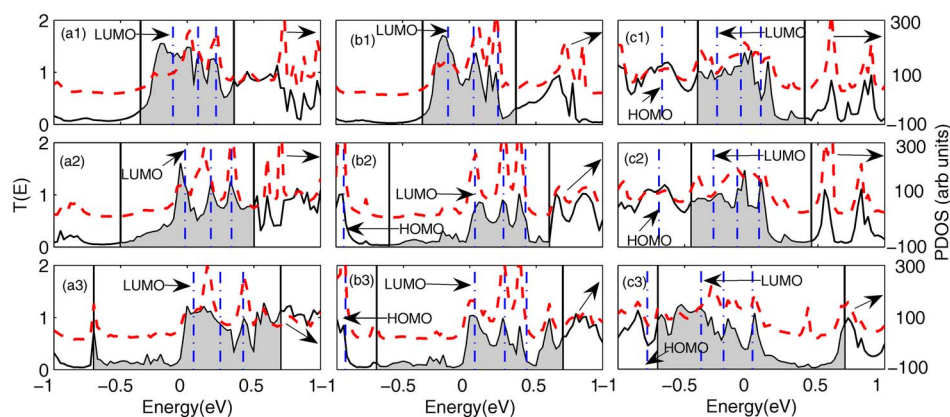


FIG. 3. (Color online) (a1)–(a3), (b1)–(b3), and (c1)–(c3) describe the transmission coefficient and the corresponding PDOS at different bias voltages for the systems  $M1$ ,  $M2$ , and  $M4$ , respectively. (a1)–(a3) correspond to the bias voltages being 0.7, 1.0, and 1.4 V; (b1)–(b3) correspond to the bias voltages being 0.7, 1.2, and 1.4 V; and (c1)–(c3) correspond to the bias voltages being 0.8, 0.9, and 1.4 V, respectively. The region between two solid lines is the bias window, and the shaded area denotes the integral area of the bias window.

spectra also present much different behavior from those presented in  $M1$ – $M4$ . The reason for it is due to the fact that the structure and the contacting position of the  $C_{60}$  molecule are different from other four structures, as shown in Fig. 1(b).

In order to explain the NDR behavior, in Figs. 3(a)–3(c), we plot the transmission coefficient and the corresponding PDOS for  $M1$ ,  $M2$ , and  $M4$  under different bias voltages. From Fig. 3(a1), it is found that at the bias  $V_b = 0.7$  V, the wide valley with very small transmission coefficient in the energy region between HOMO and LUMO is just lying on the left edge of the integral window and does not enter into the integral window. When the bias voltage has taken the value between  $V_b = 0.7$  V and  $V_b = 1.0$  V, the bias window is increased with the bias voltage, but the wide valley enters into the integral window and factually the total integral area gets smaller. As a result, the current is decreased and NDR appears. From Fig. 3(a3), we find that when the bias voltage is further increased, other integral area enters the bias window and the current increases again and NDR disappears. From Figs. 3(b1)–3(b3), we can find that a small deformation of the  $C_{60}$  molecule can increase the peak-to-valley ratio of NDR and the bias voltage range where NDR appears. This is due to the fact that a more wide transmission valley with very small transmission coefficient enters the bias window and the integral area gets smaller. However, from Figs. 3(c1)–3(c3), it can be found that when the compression is further reinforced, the transmission valley is replaced by transmission peaks. Therefore, peak-to-valley ratio becomes small. It is well known that the transmission coefficient is related to the coupling degree between molecular orbitals and the incident states from the electrodes, and so the change in the integral area is due to the change in the coupling degree between the molecule and the electrodes. The deformation of the  $C_{60}$  molecule can lead to the shift of the molecular orbitals and so change the coupling degree between the molecule and the electrodes.

In summary, the calculated results show that NDR behavior can be found at a certain bias voltage range for ideal  $C_{60}$  molecule devices. Small deformation of the  $C_{60}$  molecule can increase the peak-to-valley ratio. When the compression is further reinforced, the peak-to-valley ratio will be gradually weakened and at last the NDR disappears. We suggested that the shift of the wide transmission valley with very small transport coefficient between HOMO and LUMO in the bias window at different bias voltages is the origin of the NDR.

This work was supported by the National Natural Science Foundation of China (Nos. 90403026 and 10674044), by the Ministry of Science and Technology of China (No. 2006CB605105 and 2007CB310500), by Hunan Provincial Natural Science Foundation of China (Nos. 06JJ20004 and 07JJ107), and by the Program for New Century Excellent Talents in University.

- <sup>1</sup>R. P. Andres, T. Bein, M. Dorogi, S. Feng, J. I. Henderson, C. P. Kubiak, W. Mahoney, R. G. Osifchin, and R. Reifenberger, *Science* **272**, 1323 (1996).
- <sup>2</sup>T. R. Kelly, H. D. Silva, and R. A. Silva, *Nature (London)* **401**, 150 (1999).
- <sup>3</sup>J. Chen, M. A. Reed, A. M. Rawlett, and J. M. Tour, *Science* **286**, 1550 (1999); J. Chen, W. Wang, M. A. Reed, A. M. Rawlett, D. W. Price, and J. M. Tour, *Appl. Phys. Lett.* **77**, 1224 (2000).
- <sup>4</sup>D. I. Gittins, D. Bethell, D. J. Schiffrin, and R. J. Nichols, *Nature (London)* **408**, 67 (2000).
- <sup>5</sup>L. L. Chang, L. Esaki, and R. Tsu, *Appl. Phys. Lett.* **24**, 593 (1974).
- <sup>6</sup>Z. K. Tang and X. R. Wang, *Appl. Phys. Lett.* **68**, 3449 (1996).
- <sup>7</sup>X. R. Wang and Q. Niu, *Phys. Rev. B* **59**, R12755 (1999).
- <sup>8</sup>X. R. Wang, Y. P. Wang, and Z. Z. Sun, *Phys. Rev. B* **65**, 193402 (2002).
- <sup>9</sup>J. M. Seminario, A. G. Zacarias, and J. M. Tour, *J. Am. Chem. Soc.* **122**, 3015 (2000).
- <sup>10</sup>J. Cornil, Y. Karzazi, and J. L. Bredas, *J. Am. Chem. Soc.* **124**, 3516 (2002).
- <sup>11</sup>J. Taylor, M. Brandbyge, and K. Stokbro, *Phys. Rev. B* **68**, 121101 (2003).
- <sup>12</sup>M. Q. Long, K. Q. Chen, L. L. Wang, B. S. Zou, and Z. Shuai, *Appl. Phys. Lett.* **91**, 233512 (2007).
- <sup>13</sup>M. D. Ventra, S. G. Kim, S. T. Pantelides, and N. D. Lang, *Phys. Rev. Lett.* **86**, 288 (2001).
- <sup>14</sup>Y. Luo, C. K. Wang, and Y. Fu, *J. Chem. Phys.* **117**, 10283 (2002).
- <sup>15</sup>R. Liu, S. H. Ke, H. U. Baranger, and W. Yang, *J. Am. Chem. Soc.* **128**, 6274 (2006).
- <sup>16</sup>L. Chen, Z. P. Hu, A. D. Zhao, B. Wang, Y. Luo, J. L. Yang, and J. G. Hou, *Phys. Rev. Lett.* **99**, 146803 (2007).
- <sup>17</sup>X. F. Li, K. Q. Chen, L. L. Wang, M. Q. Long, B. S. Zou, and Z. Shuai, *Appl. Phys. Lett.* **91**, 133511 (2007).
- <sup>18</sup>H. W. Kroto, J. R. Heath, S. C. O'Brien, R. F. Curl, and R. E. Smalley, *Nature (London)* **318**, 162 (1985).
- <sup>19</sup>C. Joachim, J. K. Gimzewski, R. R. Schlittler, and C. Chavy, *Phys. Rev. Lett.* **74**, 2102 (1995).
- <sup>20</sup>H. K. Park, J. W. Park, A. K. L. Lim, E. H. Anderson, A. P. Alivisatos, and P. L. McEuen, *Nature (London)* **407**, 57 (2000).
- <sup>21</sup>C. G. Zeng, H. Q. Wang, B. Wang, J. L. Yang, and J. G. Hou, *Appl. Phys. Lett.* **77**, 3595 (2000).
- <sup>22</sup>J. Taylor, H. Guo, and J. Wang, *Phys. Rev. B* **63**, 121104(R) (2001).
- <sup>23</sup>J. J. Palacios, *Phys. Rev. B* **72**, 125424 (2005).
- <sup>24</sup>N. Sergeev, A. A. Demkov, and H. Guo, *Phys. Rev. B* **75**, 233418 (2007).
- <sup>25</sup>C. Joachim, J. K. Gimzewski, and A. Aviram, *Nature (London)* **408**, 541 (2000).
- <sup>26</sup>M. Brandbyge, J. L. Mozos, P. Ordejon, J. Taylor, and K. Stokbro, *Phys. Rev. B* **65**, 165401 (2002).